



AFRL-RX-WP-TM-2010-4126

**COLLABORATIVE RESEARCH AND DEVELOPMENT
(CR&D)**

**Delivery Order 0046: Structure-Processing-Property Relationships of
Adaptive Polymer Nanocomposites**

Hilmar Koerner

Universal Technology Corporation

NOVEMBER 2007

Final Report

Approved for public release; distribution unlimited.

See additional restrictions described on inside pages

STINFO COPY

**AIR FORCE RESEARCH LABORATORY
MATERIALS AND MANUFACTURING DIRECTORATE
WRIGHT-PATTERSON AIR FORCE BASE, OH 45433-7750
AIR FORCE MATERIEL COMMAND
UNITED STATES AIR FORCE**

NOTICE AND SIGNATURE PAGE

Using Government drawings, specifications, or other data included in this document for any purpose other than Government procurement does not in any way obligate the U.S. Government. The fact that the Government formulated or supplied the drawings, specifications, or other data does not license the holder or any other person or corporation; or convey any rights or permission to manufacture, use, or sell any patented invention that may relate to them.

This report was cleared for public release by the USAF 88th Air Base Wing (88 ABW) Public Affairs Office (PAO) and is available to the general public, including foreign nationals. Copies may be obtained from the Defense Technical Information Center (DTIC) (<http://www.dtic.mil>).

AFRL-RX-WP-TM-2010-4126 HAS BEEN REVIEWED AND IS APPROVED FOR PUBLICATION IN ACCORDANCE WITH THE ASSIGNED DISTRIBUTION STATEMENT.

*//Signature//

MARK N. GROFF
Project Engineer
Business Operations Branch
Integration and Operations Division

//Signature//

KENNETH A. FEESER
Chief
Business Operations Branch
Integration and Operations Division

This report is published in the interest of scientific and technical information exchange, and its publication does not constitute the Government's approval or disapproval of its ideas or findings.

*Disseminated copies will show “//Signature//” stamped or typed above the signature blocks.

REPORT DOCUMENTATION PAGE					Form Approved OMB No. 0704-0188	
<p>The public reporting burden for this collection of information is estimated to average 1 hour per response, including the time for reviewing instructions, searching existing data sources, gathering and maintaining the data needed, and completing and reviewing the collection of information. Send comments regarding this burden estimate or any other aspect of this collection of information, including suggestions for reducing this burden, to Department of Defense, Washington Headquarters Services, Directorate for Information Operations and Reports (0704-0188), 1215 Jefferson Davis Highway, Suite 1204, Arlington, VA 22202-4302. Respondents should be aware that notwithstanding any other provision of law, no person shall be subject to any penalty for failing to comply with a collection of information if it does not display a currently valid OMB control number. PLEASE DO NOT RETURN YOUR FORM TO THE ABOVE ADDRESS.</p>						
1. REPORT DATE (DD-MM-YY) November 2007		2. REPORT TYPE Final		3. DATES COVERED (From - To) 08 December 2005 – 29 November 2007		
4. TITLE AND SUBTITLE COLLABORATIVE RESEARCH AND DEVELOPMENT (CR&D) Delivery Order 0046: Structure-Processing-Property Relationships of Adaptive Polymer Nanocomposites				5a. CONTRACT NUMBER F33615-03-D-5801-0046		
				5b. GRANT NUMBER		
				5c. PROGRAM ELEMENT NUMBER 62102F		
6. AUTHOR(S) Hilmar Koerner				5d. PROJECT NUMBER 4349		
				5e. TASK NUMBER L0		
				5f. WORK UNIT NUMBER 4349L0VT		
7. PERFORMING ORGANIZATION NAME(S) AND ADDRESS(ES) Universal Technology Corporation 1270 North Fairfield Road Dayton, OH 45432-2600				8. PERFORMING ORGANIZATION REPORT NUMBER S-531-046		
9. SPONSORING/MONITORING AGENCY NAME(S) AND ADDRESS(ES) Air Force Research Laboratory Materials and Manufacturing Directorate Wright-Patterson Air Force Base, OH 45433-7750 Air Force Materiel Command United States Air Force				10. SPONSORING/MONITORING AGENCY ACRONYM(S) AFRL/RXOB		
				11. SPONSORING/MONITORING AGENCY REPORT NUMBER(S) AFRL-RX-WP-TM-2010-4126		
12. DISTRIBUTION/AVAILABILITY STATEMENT Approved for public release; distribution unlimited.						
13. SUPPLEMENTARY NOTES PAO Case Number: 88ABW 2010-1204; Clearance Date: 16 Mar 2010. Report contains color. Research was completed in 2007.						
14. ABSTRACT This research in support of the Air Force Research Laboratory Materials and Manufacturing Directorate was conducted at Wright-Patterson AFB, Ohio. This research developed methods to fabricate polymer nanocomposites and determined the structure-processing-property relationships to enable optimization of polymer nanocomposites with adaptive mechanical and electromagnetic properties for future UAV systems.						
15. SUBJECT TERMS adaptive polymer nanocomposites, uniaxial deformation						
16. SECURITY CLASSIFICATION OF:			17. LIMITATION OF ABSTRACT: SAR	18. NUMBER OF PAGES 16	19a. NAME OF RESPONSIBLE PERSON (Monitor) Mark N. Groff	
a. REPORT Unclassified	b. ABSTRACT Unclassified	c. THIS PAGE Unclassified			19b. TELEPHONE NUMBER (Include Area Code) N/A	

I) Transient Microstructure of low hard-segment thermoplastic polyurethane under uniaxial deformation.

Microstructure evolution during uniaxial deformation ($\lambda=1$ to $\lambda=3.5$) of a low hard segment (<10mol%) thermoplastic polyurethane (LHS-TPU) has been followed by in-situ wide angle X-ray (WAX) and small angle X-ray (SAX) with a focus on identifying the peculiar structural changes associated with features in its tensile behavior. For the LHS-TPU, a unique transient lamellar morphology with tilted crystallites is observed at elongations up to 100% ($\lambda=2$) resulting in a 4-point pattern in the SAX. These soft segment crystallites exhibit a unit cell that is iso-structural to Poly(butyleneadipate) (PBA). Owing to the cylindrical symmetry of the deformation, the distinct morphology with tilted crystallites can be modeled in 2D by a simple packing of lines resembling lamellar crystallites. The hard segments, due to their low content only act as physical crosslinks and do not crystallize. The morphology changes correspond to onset of yield stress and strain hardening in the stress-strain behavior during uniaxial elongation. Further elongation leads to a conventional 2-point pattern along the deformation direction with lamellar crystallites aligning in the plane normal to the deformation. Figure 1 summarizes data from SAX, WAX and image analysis. A transient morphological structure was discovered by in-situ X-ray. The transition from an equatorial 4 point pattern to a meridional 2 point pattern has not been observed in such system.

Thermoplastic elastomers have been prepared and characterized via SAX and WAX experiments in in-situ tensile tests to shed light into the morphology development of carbon nanotube filled systems. The neat PU system shows a transient morphology at low strains. DSC, NMR and X-ray indicate that Irogran is very similar in its behavior as poly (butylene adipate) and differences can be accounted for the low content of physical crosslinks. A small amount of crystallites present in the as-made sample (phase I) leads to a chevron-type morphology upon small deformations ($\lambda<1.9$) with the appearance of a figure eight pattern in SAX. Further stretching of the samples leads to a typical lamellar morphology with lamellar crystallites perpendicular to the stretching direction (phase II). Extreme elongation leads to a fibrillar morphology. Only a detailed study of the deformation behavior of this system reveals features that are otherwise overlooked. The unique 4-point pattern caused by chevron-type morphology of already present crystallites can be modeled adequately by schematic lines that represent crystallite alignment and packing. These results are important for the understanding of nanocomposite systems that use Irogran as the matrix polymer.

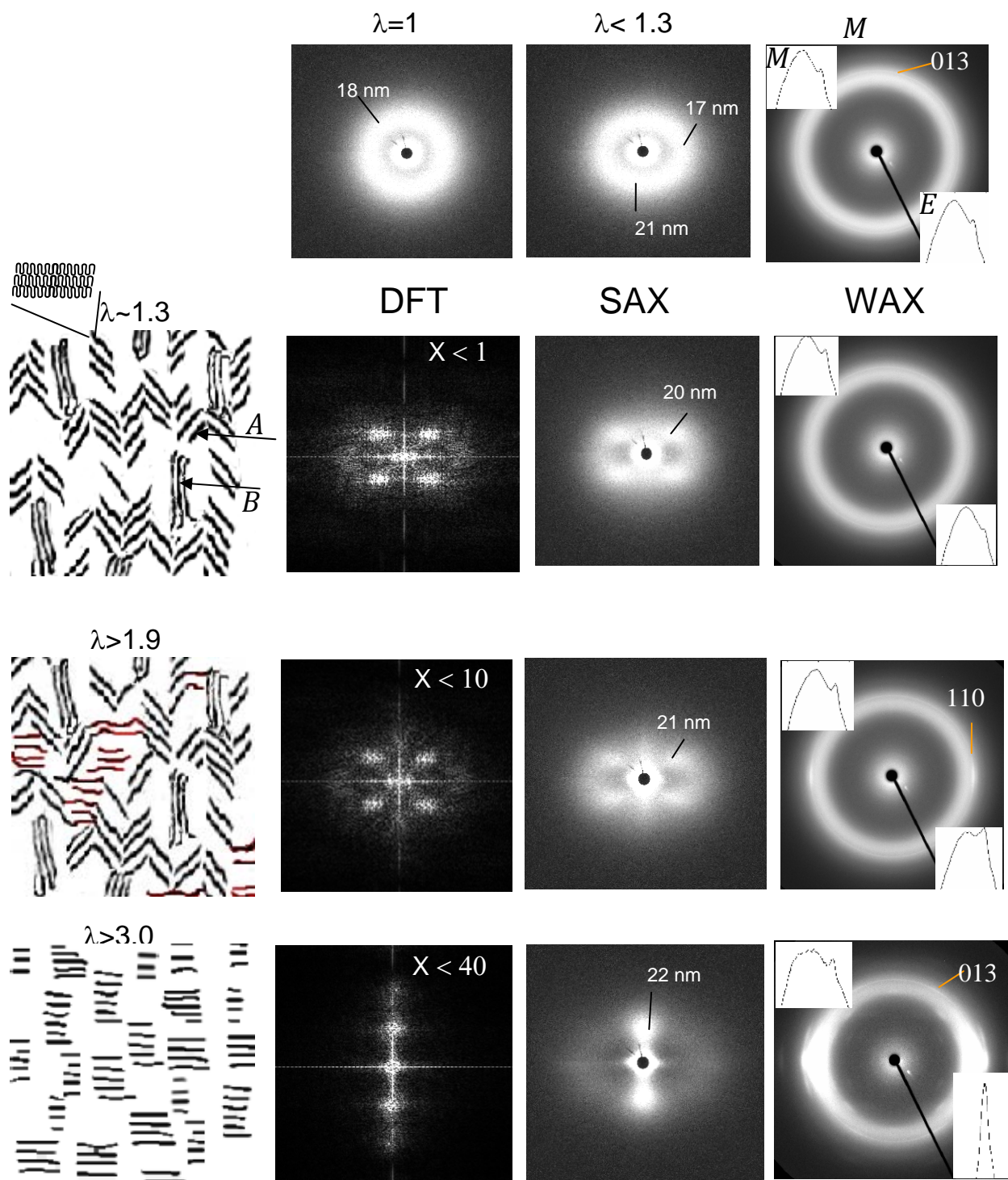


Figure 4a: Structural evolution of SAX pattern and Digital Fourier transformation of morphology model.

WAX & SAX patterns of neat PU upon deformation and schematic representation of morphology. a) 2D WAX pattern with equatorial (*E*, horizontal) and meridional (*M*, vertical, elongation direction) scans as insets at $\lambda=1$, $\lambda=1.3$, $\lambda=2$, $\lambda=3.5$.

II) MORPHOLOGY-DEFORMATION CORRELATIONS IN CNT NANOCOMPOSITE ELASTOMERS

Understanding the morphological evolution and interplay of anisotropic nanofiller and matrix is important to predict properties such as conductivity and response to external fields. The response of a carbon nanotube (CNT) filled thermoplastic elastomer (PU) to external deformation was probed via in-situ X-ray measurements both in small-angle (SAX) and wide-angle (WAX) experiments to reveal morphological changes of both polymer and nanoparticle filler. Strain-induced crystallization of the PU, alignment of the amorphous and crystalline phase of the polymer and its effect on the orientation of the CNT are discussed as a function of strain-rate and filler concentration. It is found that the CNT concentration plays a major role in the mechanical properties as well as the alignment and crystallization of the matrix polymer, while the rate at which the system is deformed only affects the morphological evolution to a minor degree. The addition of carbon nanotubes masks the differences in the strain rate found for the neat PU system. The degree of alignment for CNTs is much smaller than predicted from a pure kinematic perspective. Possible entanglements and the flexibility of the CNTs lead to an orientation that is independent of concentration.

Figure 2 shows data from in-situ X-ray measurements on filled CNT/PU samples. Figure 3 a) shows plateau of crystallite orientation, b) strain when strain hardening is observed. Figure 4 shows crystallinity as a function of strain rate and concentration.

Figure 5 demonstrates that CNT loading does not affect the alignment ability of the individual tubes in the nanocomposites.

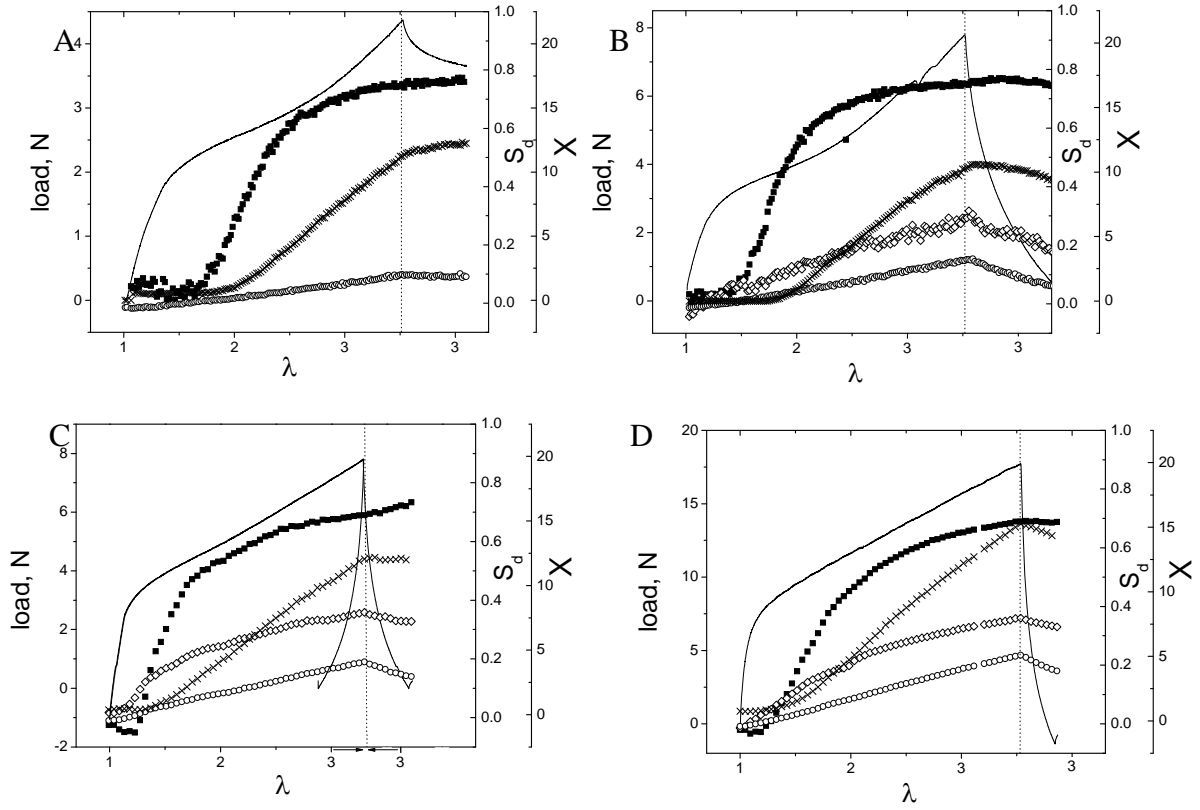


Figure 2: Tensile data (line), crystallinity index (x), Hermans orientation parameter for crystalline PU (filled squares), amorphous PU (circles) and CNT (open diamonds) for A) a neat PU sample, B) a 1% CNT/PU sample and C) a 10wt% CNT/PU sample D) a 20% CNT/PU sample at 1mm/min strain rate.

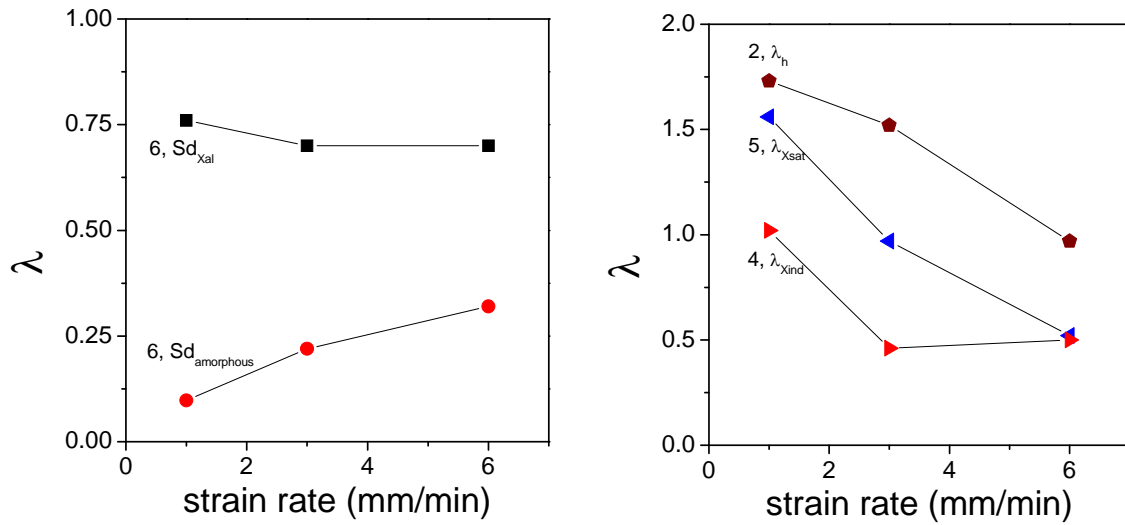


Figure 3: a) Plateau of crystallite orientation. b) Strain when strain hardening is observed.

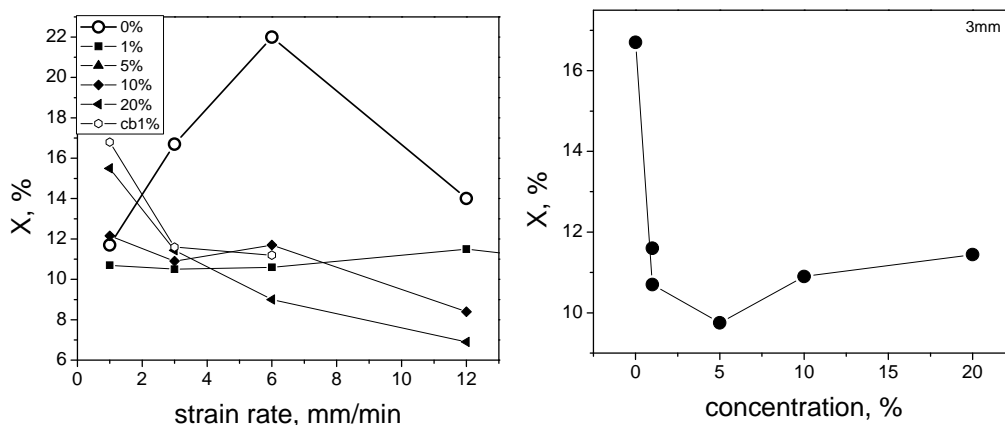


Figure 4: a) Crystallinity of PU system at maximum strain. b) Crystallinity as a function of concentration at 3mm/min strain rate.

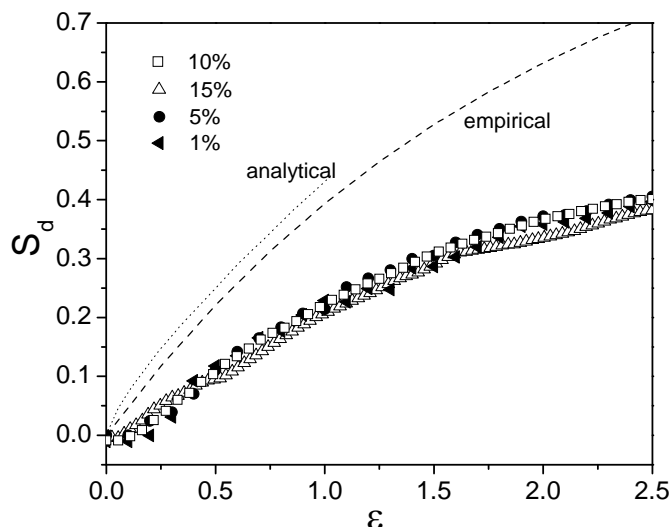


Figure 5: CNT orientation parameter S_d for 1, 5, 10 and 15wt% PU/CNT nanocomposites with example tensile data for the 1 and 15wt% samples. The dashed line represents a fit for ideal kinematic alignment of a rod. Tube loading does not play a role in the final orientation parameter of CNTs. Independent of strain rate; tubes align the same way at high or low concentrations.

In summary, a complex interplay between nucleation and strain induced crystallization, polymer crystallite orientation and tube alignment underlie the reinforcing effect of multi-wall CNT on Irogran. Incorporation of as little as 2.9 vol% of CNTs into the thermoplastic polyurethane increases yield stress, stress at break and modulus, without losing the ability to stretch the elastomer above 1000%. These properties are influenced by a strain induced crystallization of the soft-segments of the PU, which leads to a complex synergism in the mechanical reinforcement of PU nanocomposites. This synergism also carries over to the alignment of CNTs during deformation.

III) Growth Mechanism of Gold Nanoparticles and Colloidal Crystals Studied by in-situ SAXS

Gold nanoparticles have long been around, since ancient times from the Lycurgus Cup¹ to medieval stained glass, to modern times with the Turkevich synthesis² in the early 1950's (old by modern standards) and the Brust-Schiffrin synthesis³ of the mid 1990's. More recently, a one-pot, easily scalable, low polydispersity nanoparticle synthesis route was developed by Stucky and colleagues at UCSB⁴. Like the Brust method, the Stucky method provides sizes smaller than typically achieved in the Turkevich method, however it is one-phase and one-pot unlike the Brust method.

TEM, in-situ UV-Vis, in-situ SAXS combined to give physical data of different perspectives. UV-Vis provides concentration of gold atoms bound into nanoparticles from Beer-Lambert's law and Mie theory based on the absorption of the surface plasmon resonance located near 520nm, while the specific wavelength of the surface plasmon provides limited information about the nanoparticle size. TEM provides a physical size measurement. SAXS studies provide number density of nanoparticles and the size of the nanoparticles as their nucleation and growth in size occurs, and recent studies have suggested its utility in understanding nanoparticle growth mechanisms. These techniques combine to help answer broader questions about the mechanism of nanoparticle growth.

SAXS

Evolution of Au nanoparticle synthesis was followed using synchrotron X-ray experiments, conducted at X27C, National Synchrotron Light Source at Brookhaven National Laboratory. Sample to detector distance was 2000 mm at a wavelength of 0.1371nm, defined by a double multi-layer monochromator. The synchrotron x-rays were collimated to a 600 μ m beam size using a three-pinhole collimator³¹. SAX images were obtained using a Mar CCD detector. Stock solutions of Au precursor/thiol surfactant and reducing agent in benzene were mixed in the appropriate stoichiometry right before the reaction. The mixture was thoroughly mixed in a small vial and immediately filled into the reaction cell. The time between initial mixing and the first exposure was about 2 minutes. The sealed reaction cell was mounted into the beam and image collection followed with 4 minutes exposure time for each frame. The reactions were run for 1-6 hours depending on the ratio of reducing agent to Au precursor. The collected images were corrected for background and initial beam intensity as outlined in the next chapter.

Data reduction

Dark current correction and de-zingering of the 2d detector data was done internally while capturing the data on the MarCCD detector. Further correction of raw intensity data (Sa2D) was done by normalizing to beam intensity I0 (initial intensity of beam as it enters the sample changes over time due to beam fluctuations, filling ring), transmission T (sample transmission is obtained via normalizing measurements from photodiodes before and after the sample (I0/I0ef) with respect to empty cell data – EF2D)

$$\frac{1}{I_0} \times \left(\frac{1}{T} \times (Sa2D) - \frac{I_0}{I_{ef}} \times (EF2D) \right)$$

Experiments were reproducible. Intensity data from two different reactions essentially fall on top of each other (example C12, 1:1 can show in supplemental). A matrix of reactions was run varying the molar ratio of reducing agent towards Au precursor (5:1, 1:1, 0.5:1) in addition to changing the capping agent (C8, C12, C16 thiol). Only four of these are shown here to demonstrate the feasibility of SAXS to derive detailed information on the kinetics and evolution of particle growth (maybe others in supplemental). Reactions ran for about 1hr for 5:1 ratio and 3hrs for 1:1 ratio and 6hrs for 0.5:1 ratio.

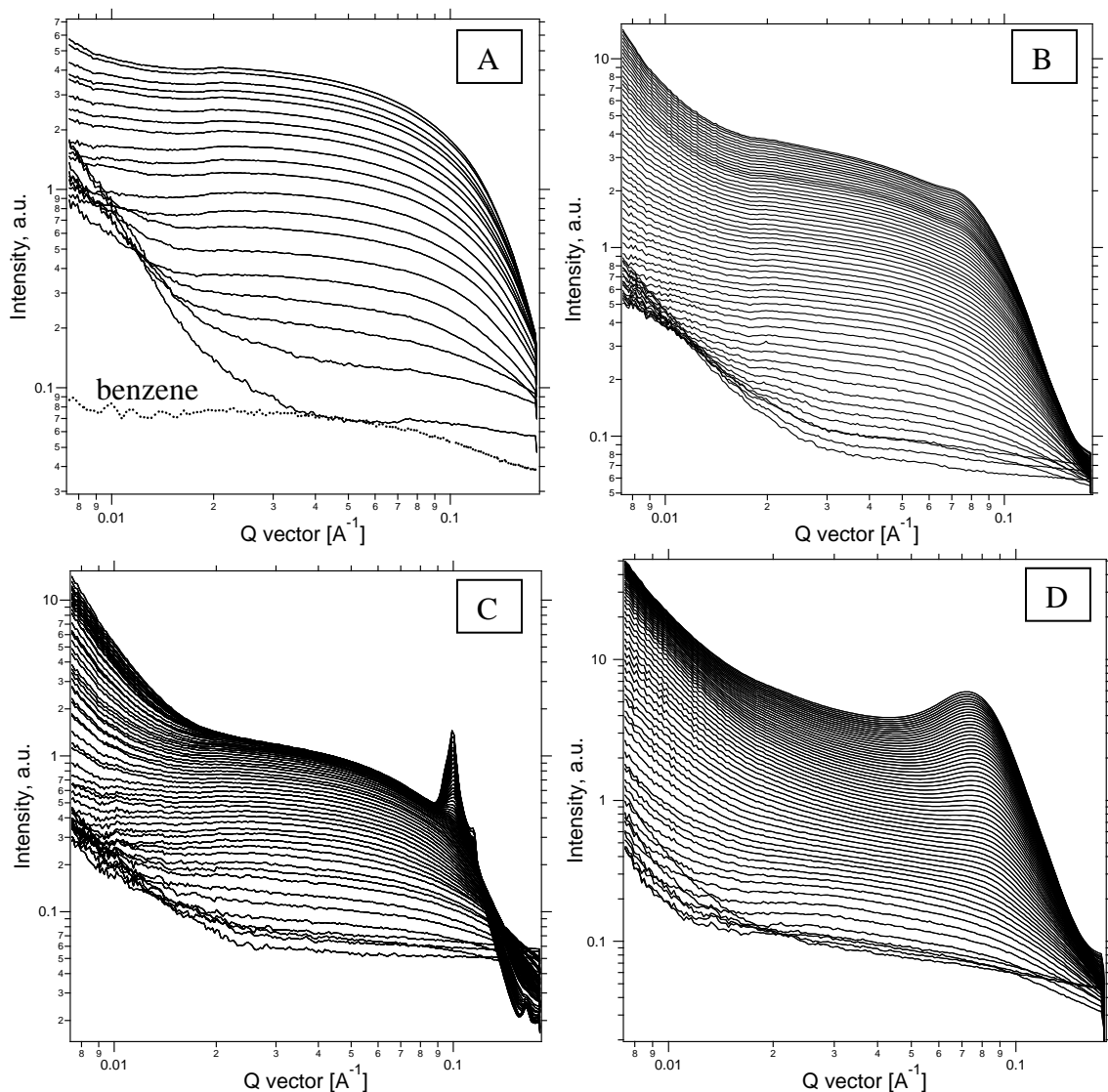


Figure 6: Reduced SAXS data for A) C12/5:1. The dotted line is from neat Benzene. B) C12/1:1; C) C8/1:1 and D) C16/1:1.

Based on findings in Figure 7, the data for these three reactions can be assumed independent of surfactant length. Only when excess reducing agent is used (C12/5:1) the reaction proceeds much quicker with basically no induction period and a steeper incline in section [II] of the reaction. Turnover into region [III] of the reaction is setting in at smaller particle sizes (3nm as opposed to 4nm for the other reactions). The slope of region [II] is the same for all three surfactants. This is in agreement with UV/VIS experiments, which shows that the kinetics of the reaction is independent of surfactant. Both UV/VIS and SAX experiments also show incoherences in the incubation time of the reaction. The rate of growth is the same but the initial period [I] is strongly dependent on a number of factors, such as dust particles, fluctuations in concentrations due to micelle formation of thiols. These results stand in contrast to the mechanism proposed by Stucky et. al in which the authors hypothesize that after a short time particles grow to their final size quickly and that the number of particles increases over time. Growth according to these findings would imply a sharp increase in particle size at early reaction times. The form factor would reach equilibrium at the same time and only the intensity would increase steadily over time. A dashed line in Figure 3 schematically represents such an event. This is clearly not the case in the reactions in this study. The size of particles increases in three parts from well below 1nm up to their final size of 5nm.

Similar results have been found by Turkevich et. al in the 50s. They find the same S-shape curve for particle growth and explain their results with the chemistry of the reaction. They describe four regions: a) induction period, b) autoaccelerating portion, c) linear region, d) decay. They observe inhomogeneities in the initial portion of the reaction by electron microscopy in the range of 20nm.

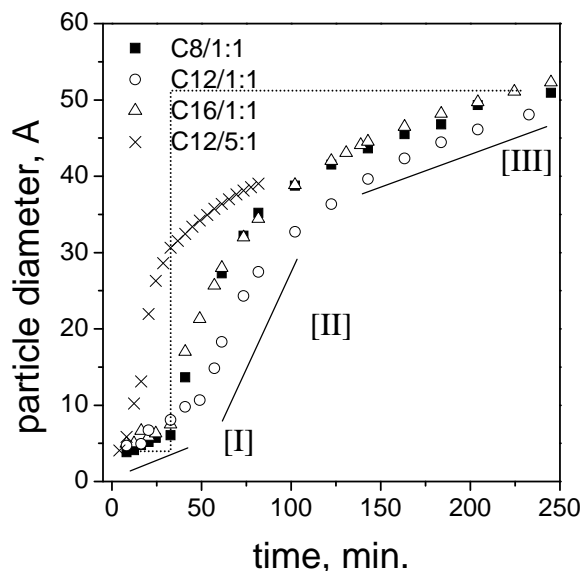


Figure 7: Particle diameter obtained from SAX fitting as a function of reaction time for C8/1:1, C12/1:1, C16/1:1 and C12/5:1.

Figure 8 demonstrates that SAX is an ideal tool to follow size distribution. A good match between TEM data and SAX of the final reaction product is shown.

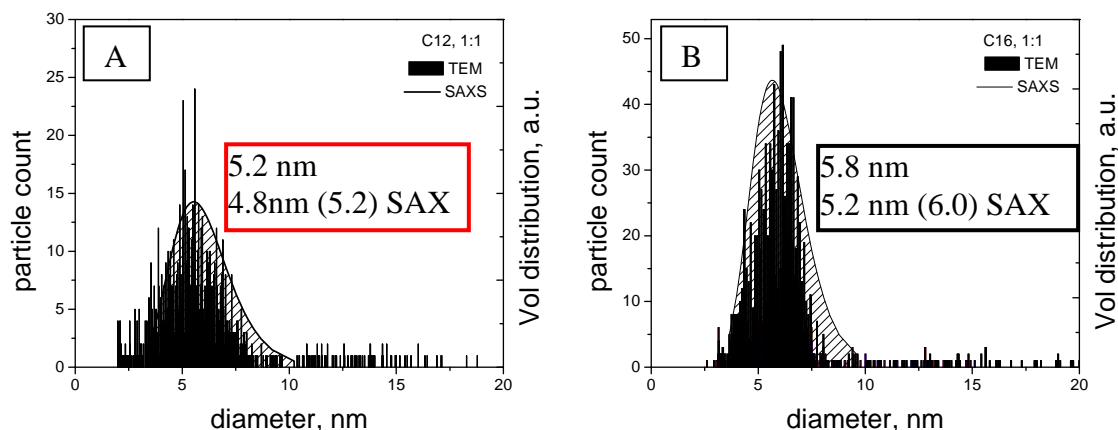
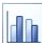



Figure 8: A) C12/1:1 and B) C16/1:1  overlaid with results from final volume distribution from SAX experiment .

Conclusions

Based on the SAX experiments and TEM analysis the following conclusions about Au nanoparticle growth in Benzene can be drawn. There is an incubation period for all reactions. Small particles form at the early stage that can be fitted with one population with a broad size distribution. A low-Q upturn at the very beginning of the reaction is indicative of micelle formation of surfactant in the solvent (confirmed by LS). The reaction progresses faster after about 30min and reaches a plateau at about 2hrs. In this region [II] the SAX data can be fitted with one population of particles with narrowing size distribution. The number of particles in this region increases. When the reaction reaches the plateau [III] the number of particles does not increase further or to a much smaller degree and the size distribution narrows. This eventually leads to the formation of colloidal crystals and the appearance of diffraction peaks on top of the sphere scattering.

These results indicate a more complicated growth mechanism compared to TEM previous TEM observations of the same reactions (Stucky paper). As opposed to particles growing quickly to their final size with further increase in number, the reactions in this study can be divided into three regimes; [I] nucleation, [II] growth and [III] ripening. SAX shows these three main areas for every reaction, independent of surfactant or reducing agent concentration. The data analysis also provides more insights into the detailed evolution within the three main regions. Noteworthy are the initial inhomogeneities due to micelle formation of thiol surfactant in benzene, possibly leading to fluctuations of Au precursor at the initial reaction step as well (Fig. 9a); coalescence of smaller particles (Fig. 9c, increase in slope in Figure 7); ripening and colloid crystallization at late stages in the reaction as seen in the formation of fcc lattice peaks in the SAX curves (Fig. 9g).

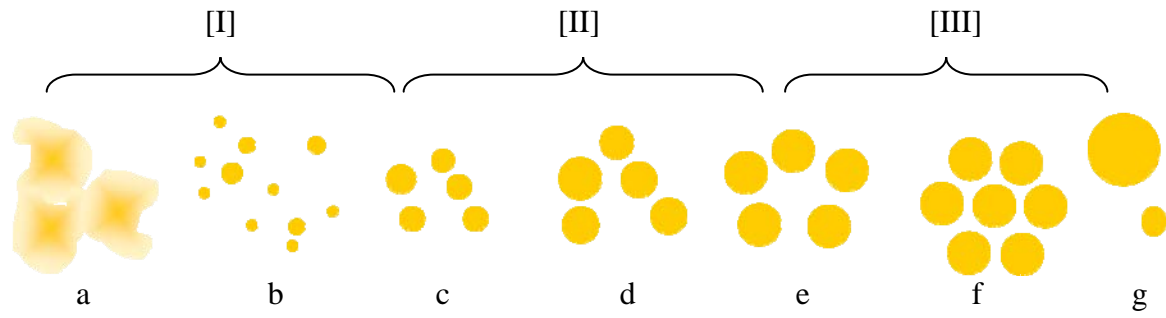


Figure 9: Schematic of possible Au nanoparticle growth. A) atomic concentration inhomogeneities, b) nucleation, c) coalescence, d) growth, e) distribution narrowing (ripening), f) colloid crystallization